concentration dependence and was slightly higher than in the control. The amounts of IL-1β and M-CSF release from macrophages were also increased for the MECNC concentrations that exceeded 1ppm. These tendencies were similar to that of the TNF-α release.

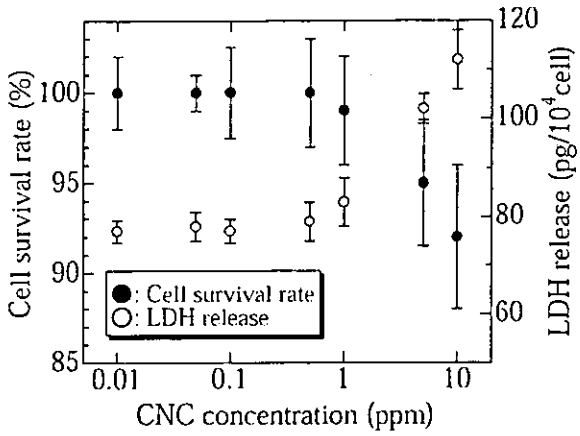

Fig. 2

The survival rate of rat fibroblasts was decreased with the addition of MECNCs for concentrations higher than 1ppm. The amounts of LDH release and cytokines release were also increased for the MECNCs at concentrations exceeding 1ppm. LDH is released from cells after cell damage and death. Cytokines are the chemical mediators within the various cells related to the immunological and inflammatory reactions of the cells. Therefore, the toxicity of MECNCs would be quite low in the lower concentration less than 1ppm.

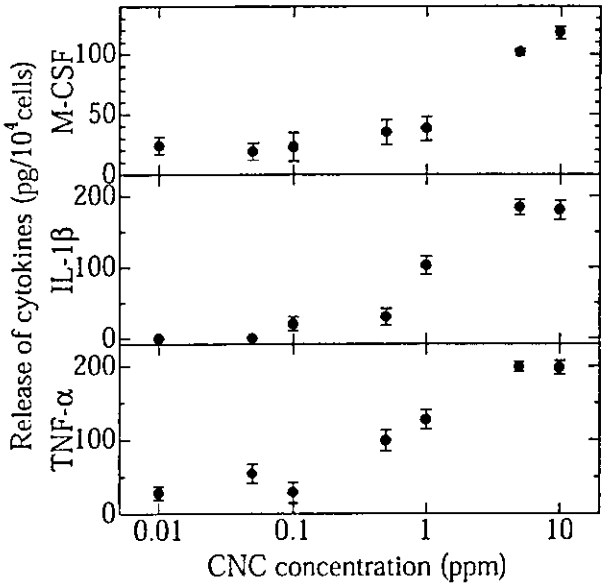

Fig. 3

PO5

Paramecium as a Model organism for Bioassay of Cytotoxicity and Biocompatibility of CNF

Nobuyuki Haga[1] and Koichi Haneda[2]

[1]Department of Biological Engineering and [2]Department of Information and Electronics, Ishinomaki Senshu University, Ishinomaki, Japan

Carbon nanofibers (CNF) whose constituent is known as carbon nanotubes are a recent technological advance for a wide variety of nano-engineering fields including biomedicine. However, little is known about the environmental effects of CNF, or its potential danger to human health. To elucidate the safety of CNF, we have examined *Paramecium* as a model organism for bioassay of cytotoxicity and biocompatibility of CNF.

Paramecium, a eukaryotic unicellular organism living in fresh water, is considered a model system of vegetative growth[1], post-mitotic cell differentiation[2] and cellular aging. *Paramecia* ingest both soluble molecules and insoluble particles by phagocytosis. Because they share common mechanisms of gene replication and expression to multicellular eukaryotic organisms and show very stable cellular functions such as phagocytosis, proliferation and cell motility, they provide a precise bioassay system in which to evaluate the cytotoxicity of environmental and ingested nanoparticles. We have established a standard experimental system that enables microliter-sized assays.

Our results show that CNF is ingested and concentrated by *Paramecium* as efficiently as nutritive bacteria revealing a means by which CNF could be introduced into the food webs of aquatic ecosystems. CNF does not affect post-mitotic cell survival at concentrations of tens of micrograms per microliter but reversibly affects cell viability in the presence of nutritive bacteria at concentrations of nanograms per microliter. The cytotoxicity of CNF suggests the interaction between CNF and metabolic products produced by digestion of bacteria, which may in turn cause cell death. Our results suggest that CNF have high potential for in vivo applications, if the concentration of CNF and co-existing metabolites are properly controlled.

PO6

Contribution of Ag Layer to the IEPM Bending Induction

Hirohisa Tamagawa and Fumio Nogata
Department of Human and Information Systems, Gifu University

1. Introduction

Membrane type polymer actuator has been a highly attractive research topic for more than a decade [1-5]. For instance, a metal plated ion exchange polymer membrane called Nafion (DuPont, U.S.A) was found to exhibit a fast and large bending upon a small applied voltage, when it is in the hydrated state [1-6]. (Hereafter ion exchange polymer membrane is called IEPM for short.) However, nobody has come by a practically usable IEPM actuator to this day due to its insufficient properties for instance, concerning Nafion IEPM actuator, the low bending controllability, the occurrence of bending relaxation, the short longevity, the low generated force, and etc.

Another type of IEPM called Selemion (Asahi glass, Co. Ltd., Japan) containing the imobile anionic functional groups exhibits bending upon a small applied voltage like Nafion, when it is metal plated and hydrated. However, still the serious difficulties such as the low bending controllability and etc have remained.

Recently, we found that the dehydration treatment on the Ag-plated Selemion and Nafion add them excellent bending controllability and longer longevity under the condition of employing the alternate voltage not the constant voltage [7]. Taken up an experimental fact from ref.[7], the dehydrated Selemion bending direction and curvature are quite precisely controlled upon the alternate applied voltage, although the hydrated Selemion exhibits merely an extremely poor controllability. Furthermore, the dehydrated Selemion longevity is quite long, and it oscillates for more than 600(s) in accordance with the alternate applied voltage with 0.2(Hz) frequency, although the hydrated one's longevity could not be beyond even a few minutes, where our definition of longevity is the duration time that IEPM can meet the following two requirements: i) the visibly large enough bending curvature change of IEPM actuator can be induced within 30(s) after reversing the polarity of voltage applied on it and ii) the bending curvature of IEPM actuator can be well controlled by the control of applied voltage polarity. Certainly, the dehydration treatment is a quite effective method for the improvement of IEPM actuator properties. However, our latest investigation found that the long application of constant voltage to the dehydrated Selemion largely shortens its longevity. It is serious issue standing against the realization of a practical IEPM actuator.

In this paper, we deal with the essential factor in need for the longevity elongation of dehydrated IEPM actuator especially Selemion and suggest the quite promising design for the practical IEPM actuator.

2. Specimen preparation

The top and bottom surfaces of Selemion containing -COOH groups were plated with silver

through the silver mirror reaction, the detail procedure is described in ref.[6]. These silver layers serve as flexible electrodes. Through this plating process, Selemion became highly hydrated, then it was placed in the sealed box in the vacuum state with a desiccant till it got highly dehydrated. This Selemion is designated as **Sel-A**.

3V constant voltage was applied to **Sel-A** with changing the voltage polarity every 3 minutes totally for 12 minutes, subsequently, 3V constant voltage was applied to it continuously for 15 minutes without polarity change. Such long application of voltage resulted in the highly curved **Sel-A**, and at the same time this process inactivated **Sel-A** bending ability, namely such **Sel-A** became extremely less deformable even the voltage is applied again, in other words, the longevity of **Sel-A** became quite short. So the relatively long application of constant voltage on **Sel-A** causes the problem of short longevity. This largely inactivated (or short longevity) **Sel-A** was straightened by applying 3V constant voltage of opposite polarity for a long while. The resulting largely inactivated **Sel-A** is hereafter called **Sel-A0**. **Sel-A0** was further treated accordingly to the requirements in need for the individual tests, then it was cut into the strip shape of dimension 20mm ×2mm × 0.2mm.

3. Experiment

Time dependence of bending curvature of strip shape Selemion IEPM actuator was measured as a function of time with a laser displacement meter. The displacement data was later converted into the curvature with a simple calculation [6].

4. Results and Discussions

4.1. Sel-A (dehydrated-silver-plated Selemion)

First of all, we'd like to show the photos of bending behavior of ordinary Selemion (**Sel-A**) in Figure 1. **Sel-A** was cut into the strip shape of dimension 20mm ×2mm × 0.2mm and horizontally clamped with electrodes as in Figure 1(a). Bear in mind that **Sel-A** is a largely (not completely) dehydrated silver plated Selemion. A visibly large enough bending curvature of **Sel-A** was observed after applying 3(V) for 180(s) as shown in Figure 1(b). Figure 2 shows the time dependence of **Sel-A** curvature upon 3V, and the quantitatively large bending curvature change is seen from this diagram.

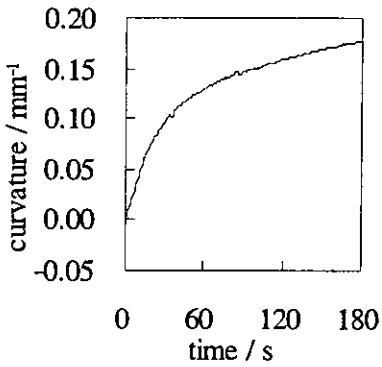

Figure 2 Time dependence of **Sel-A** curvature upon 3V

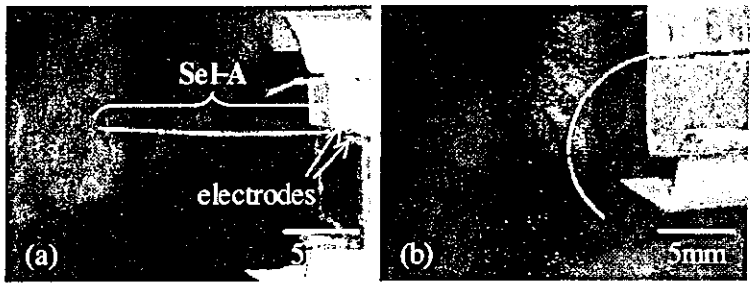

Figure 1 Side view of **Sel-A** (a) Straight **Sel-A** upon 0V (b) Curved **Sel-A** 180(s) after keeping on applying 3V

Though the detail of experimental results is not shown here, we've experimentally confirmed that **Sel-A** meets the

requirements i) and ii) suggested in the section **1. Introduction** for a long while in need for defining the longevity, as long as the applied voltage is an alternate voltage with the low frequency ~ 0.2Hz.

Those requirements are again shown here: i) the visibly large enough bending curvature change of IEPM actuator can be induced within 30(s) after reversing the polarity of voltage applied on it and ii) the bending curvature of IEPM actuator can be well controlled by the control of applied voltage polarity. We've observed that **Sel-A** has a long longevity of order at least ~ 10^3(s).

4.2. Sel-A0 (short-longevity-dehydrated-silver-plated Selemion)

As described above, the **Sel-A0** is quite largely inactivated (or has a short longevity) due to the long application of constant voltage. Figure 3 shows the time dependence of **Sel-A0** curvature upon 3V. Unlike **Sel-A** of Figure 2, **Sel-A0** never exhibits bending. So, virtually its longevity is 0(s). We speculate that it is caused by 1) the decrease of surface electric conductivity of silver layer formed on **Sel-A0** due to the long application of constant voltage on it, where we've already confirmed the decrease of surface electric conductivity of silver layer many times, or by 2) the loss of water contained in **Sel-A0** body by the water electrolysis the long application of constant voltage induced, or by both 1) and 2). In order to see actually what happened to **Sel-A0** the following experiment described in the section 4.3 was performed.

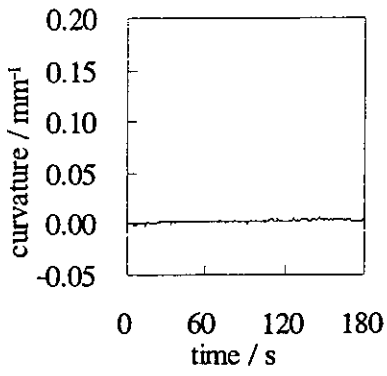

Figure 3 Time dependence of **Sel-A0** curvature upon 3V

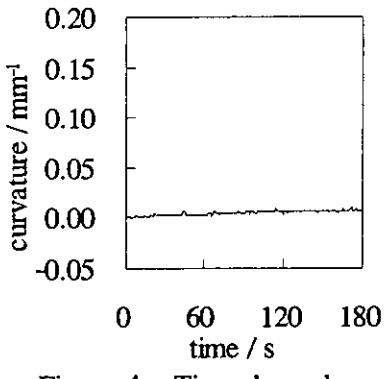

Figure 4 Time dependence of **Sel-A1** curvature upon 3V

4.3. Sel-A1 (Sel-A0 sandwiched between two gold films)

If the surface conductivity plays the critical role for the bending induction of **Sel-A0**, the raise of surface conductivity of **Sel-A0** will reactivate **Sel-A0**. Extremely thin gold films were attached on the top and bottom surfaces of **Sel-A0** by pressing them with a high pressure with a vice. The surfaces of **Sel-A0** regained the electrical conductivity. This specimen is designated as **Sel-A1**. Nothing other than gold films was used. Gold is quite inert material, and even under the applied voltage, no chemical reaction such as redox reaction occurs. It merely serves as an electric conductor. Figure 4 shows the time dependence of **Sel-A1** curvature upon 3V. Still no bending was observed, thus the longevity of **Sel-A1** is 0(s).

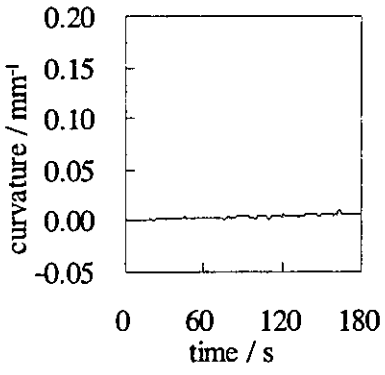

Figure 5 Time dependence of **Sel-A2** curvature upon 3V

4.4 Sel-A2 (hydrated Sel-A0)

From the results and discussions described in the sections 4.2 and 4.3, it is inevitable to suspect

that the loss of water contained **Sel-A0** inactivated **Sel-A0**. Therefore **Sel-A0** was place in the water for several minutes so as to import water molecules in it. The resulting hydrated **Sel-A0** is designated as **Sel-A2**. Figure 5 shows the time dependence of **Sel-A2** curvature upon 3V. no bending was observed after all, the longevity of **Sel-A2** is 0(s).

4.5 Sel-A3 (hydrated Sel-A0 sandwiched between two gold films

Now it is necessary to take into consideration both 1) the decrease of surface electric conductivity and 2) the loss of water molecules contained in **Sel-A0** as the cause of short longevity of **Sel-A0**. The hydrated **Sel-A0** (or **Sel-A2**) was prepared and the gold thin film was attached on its top and bottom surfaces by pressing them with a vice. Figure 6 shows the time dependence of **Sel-A3** curvature upon 3V. Bending of **Sel-A3** was observed, though the curvature was not so large as that of **Sel-A**. This result suggests that both water and surface electric conductivity are in need for the longer longevity of Selemion.

One may come to think that the silver layer may not be essential for the Selemion bending, and the use of gold film only instead of both Ag layer and gold film could serve as flexible electrodes permanently unlike silver layer, since gold is quite stable material and never involved in the reaction such as redox reaction unlike silver. However, the silver layers serve not only as electrodes but also as a bending enhancing agent. Its redox reaction caused by the applied voltage is heavily involved in the induction of effective bending of Selemion, it is detailed in ref.[8]. On this point, we performed another experiment described in the section 4.6.

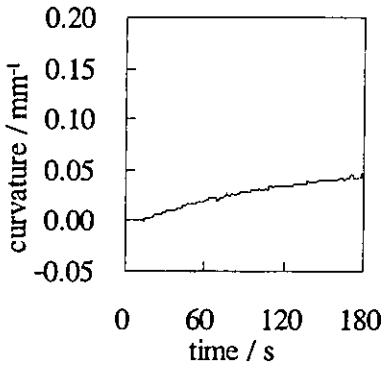

Figure 6 Time dependence of **Sel-A3** curvature upon 3V

4.6 Essential factors for the long longevity of IEPM actuators

An intact Selemion was largely dried. Its top and bottom surfaces were covered with two gold films by the same procedure employed for the preparation of **Sel-A3**. It was cut into the strip shape, dimension of 20mm ×2mm × 0.2mm. This specimen is designated as **Sel-G**. Figure 7 shows the time dependence of **Sel-G** curvature upon 3V. The bending curvature of **Sel-G** is almost 0(mm^{-1}), virtually its

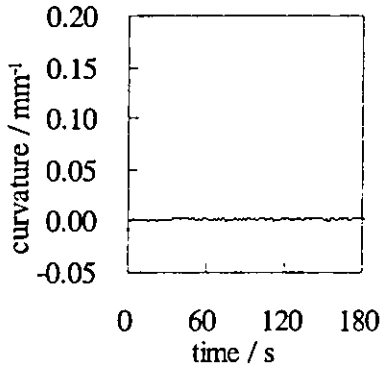

Figure 7 Time dependence of **Sel-G** curvature upon 3V

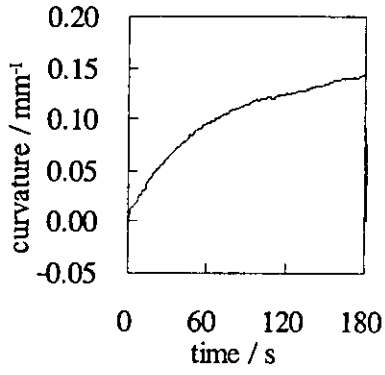

Figure 8 Time dependence of **Sel-AG** curvature upon 3V

longevity is 0(s). Next, **Sel-A** (not **Sel-A0**) whose top and bottom surfaces were covered with two gold films was prepared. It was cut into the strip shape, dimension of 20mm ×2mm × 0.2mm, and this strip was designated as **Sel-AG**. Figure 8 shows the time dependence of **Sel-AG** curvature upon 3V. A quite large bending curvature is observed. Therefore the role of Ag layer is not only serving as a flexible electrode but also inducing the bending. Namely, silver layer plays an essential role for the realization of a long longevity Selemion actuator. The similar phenomena can be seen about IEPM actuator consisting of Nafion. Figure 9 shows the time dependence of bending curvature of two IEPM actuators consisting of Nafion upon 5V (not 3V). **Naf-G** was prepared by attaching gold films on the top and bottom surfaces of largely dried Nafion. **Naf-AG** was prepared by attaching the gold films on the dried silver plated Nafion surfaces, where the silver plating procedure was the same as used for the preparation of silver plated Selemion. Existence of silver layer indeed induced the bending of IEPM of Nafion as obvious from Figure 9, At the same time, we've confirmed the longer longevity of **Naf-AG**.

To sum up, the silver layer plays a quite essential role to activate and to give a long longevity to IEPM actuators. However, the silver layer cannot sustain its role under the long application of voltage. Therefore the combinational use of silver layers and gold films is speculated to be an effective way to give IEPMs longer longevity. Indeed, the inactivated **Sel-A0** regained its bending characteristics by use of gold film as described in the section 4.5, and of course we should not forget the necessity of the minute quantity of water to be contained in IEPM, too.

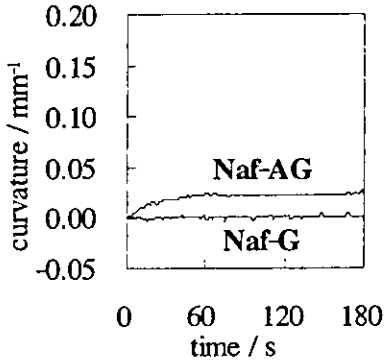

Figure 9 Time dependence of **Naf-G** and **Naf-AG** curvatures upon 3V

4.7 Design of long longevity IEPM actuator

Based on our observations described so far, we'd like to show a promising design of an IEPM actuator we think up as a long longevity IEPM actuator step by step. The fine tubular water channels are created in a certain type of IEPM body as depicted in Figure 10(a) so that a minute quantity of water can be continuously supplied. Gold wire networks are applied on the top and bottom surfaces of IEPM as depicted in Figure 10(b) so that the high surface electric conductivity is maintained. The top and bottom surfaces are plated with silver which is supposed to induce and enhance the bending of IEPM. The design of Figure 10(c) is the final one we've though up. This IEPM actuator could have a long longevity even under the constant applied voltage. Since we've yet to put this design in practice due to the technical difficulty, we've not obtained any results on the

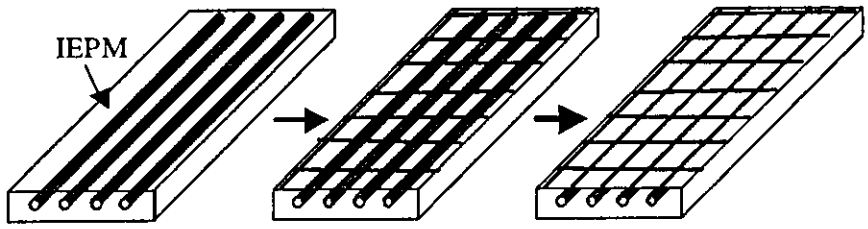

(a) water channels (b) applying gold wires (c) Ag surface plating

Figure 10 A promising design of IEPM actuator

performance of this IEPM actuator. That is our next work.

5. Conclusion

The necessity of silver layer for the induction of IEPM actuator bending has been revealed. It is actually in need not only for serving as a flexible electrode but also for elongating the IEPM actuators' longevity. At the same time, it has been strongly suggested that the minute quantity of water contained in IEPM actuator plays an essential role for the bending induction, too. We suggested a promising IEPM actuator design. Although we've not put it in practice, we can strongly expect the validity of this design backed by the experimental results shown in this paper.

References

[1] K. Oguro, Y. Kawami and H. Takenaka, Bending of an Ion-Conducting Polymer Film-Electrode Composite by an Electric Stimulus at Low Voltage, Trans. J. Micromachine Soc. 5 (1992) 27.

[2] K. Asaka, K. Oguro, Y. Nishimura, M. Mizuhara, H. Takenaka, Bending of Polyelectrolyte Membrane-Platinum Composites by Electric Stimuli I, Response Chracteristics to Various Waveforms, Polym. J. 27 (1995) 436.

[3] K. Salehpoor, M. Shahinpoor, M. Mojarrad, Actuators Made From Ion-Exchange Membrane-Metal Composites, Smart Materials Technologies, Proc. SPIE Smart Mater. Struct. San Diego, 3040 (1997) 192.

[4] M. Shahinpoor, M. Mojarrad, K. Salehpoor, Electrically Induced Large Amplitude Vibration and Resonance Characteristics of Ionic Polymeric Membrane-Metal Composites Artificial Muscles, Proc. SPIE Smart Mater. Struct. San Diego, 3041 (1997) 829.

[5] Y. Bar-Cohen, T. Xue, M. Shahinpoor, K. Salehpoor, J. Simpson, J. Smith, Low-mass muscle actuators using electroactive polymers (EAP), Proc. SPIE Smart Mater. Struct. San Diego, 3324 (1998) 218.

[6] H. Tamagawa, F. Nogata, T. Watanabe, A. Abe, K. Yagasaki, Bending curvature and generated force by Nafion actuator, IEEE ICIT'02, Bankok, (2002) 945.

[7] H. Tamagawa, and F. Nogata, Bending response of dehydrated ion exchange polymer membranes to the applied voltage, J. Membrane Sci., 243 (2004) 229.

[8] H. Tamagawa, F. Nogata, and S. Popovic, Roles of Ag redox reaction and water absorption inducing the Selemion bending, accepted in J. Membrane Sci., (2004).

PO7

Consolidation of Multi-Walled Carbon Nanotube and Application to Biomaterial

M. Omori[1], A. Okubo[2], T. Hashida[1] and K. Tohji[1]

[1]Graduate School of Engineering and [2]Institute for Materials Research, Tohoku University

A lot of investigations have been shown that CNTs exhibit many superior mechanical, electric and electronic properties over any other known material and hold substantial promise as high-strength composites, energy storage and energy conversion devices, sensors, field emission displays and radiation sources, hydrogen storage media and nanometer-sized semiconductor devices. CNT consists of single-walled carbon nanotube (SWNT), double-walled carbon nanotube (DWNT) and multi-walled carbon nanotube (MWNT). One of interests arises from their formidable mechanical properties, i.e. Young's modulus up to 640 GPa for SWNT and up to 1800 GPa for MWNT and strength up to 45 GPa for SWNT. CNT is expensive these days, but the cost of its fabrication will surely decrease in near future. Low-cost CNTs will be useful for fillers of composites and starting materials to produce structural and/or functional compacts.

Bulk density and Young's modulus of bone is less than 2.1 g/ml and 30 GPa, respectively, and there is nothing satisfying them in ceramics and metal but graphite. Strength of artificial graphite is not enough to replace bone. Materials prepared from CNT will be stronger than bone. Graphite and carbon are neither toxic nor bioactive. Bioactivity is a good factor in application replacing bone. To improve bioactivity, it is appropriate to coat a bioactive material such as haydroxyapatite.

Graphite is a hard-to-sinter material, and its powder can only be sintered at very high temperatures under pressing. The sintering ability of CNT is the same as that of graphite, and advanced techniques are needed to consolidate it at lower temperatures before transforming into graphite. The spark plasma system (SPS) has been developed for sintering of metal and ceramics in the plasma and electric field, and it has been used for consolidation of various kinds of materials such as metals, ceramics and polymers. Consolidation of the MWNT did not result in material applicable for property test. The novolak type of phenol resin was selected for consolidation additive because it is soluble in organic solvent.

The MWNT (NanoLab Inc., USA) was purified to remove metal catalysts using solution of 50% HNO_3. Phenol resin was dissolved in ethanol. The MWNTs were put in the ethanol solution. After evaporating ethanol, the phenol resin film on the MWNT was decomposed at about 200°C in air. The coated MWNTs were put in a graphite die and set in the spark plasma system (SPS) (Sumitomo Coal Mining, Japan, SPS1050). The consolidation was carried out between 1000°C and 1600°C at 120 MPa in a vacuum. In case of the consolidation at 1000°C, the consolidation temperature was raised as follows: heating rate from 0°C to 900°C at 100°C/min, from 900°C to 980°C at 20°C/min, from 980°C to 1000°C at 5°C/min and holding time at 1000°C for 5 min.

The microstructure of the consolidated MWNT was analyzed by a transmission electron microscope

(JEOL, Japan, JT-007). The polished surface of the consolidated MWNT was observed with an optical microscope (Nikon, Japan, N-01). X-ray diffraction (XRD) was carried out on the MWNT and the consolidated one using Cu Kα line by an X-ray diffractometer (Rigaku, Japan, Rotaflex, RU-200B). Density of the consolidated disk was determined based on Archimedes' principle using water. Elastic modulus of disk samples (3 mm in thickness and 20 mm in diameter) was measured by a pulse-echo overlap ultrasonic technique, using an ultrasonic detector (Hitachi Kenki Co. Ltd., Japan, ATS-100) and a storage oscilloscope (Iwasaki Tsushinki Co. Ltd., Japan, DS6411).

The consolidated MWNT was a soft compact such as pencil lead, and its bulk density was less than 1.74 g/ml. Three point bending strength of the consolidated MWNT was not measured because it was plastically deformed. The consolidated MWNT was bonded with the amorphous carbon converted from the phenol resin. High binding force would not be expected for amorphous carbon. It is necessary to find strong binders.

Coating of the consolidated MWNT was carried out using solid reaction of $CaHPO_4 \cdot 2H_2O$ (6 moles) and $Ca(OH)_2$ (4 moles). These powders were suspended in distilled water using glycolic acid. The consolidated MWNT was dipped in the suspension and dried. The coated MWNT was put in the graphite die with carbon powders and set in SPS. The coating of HA was carried out at 1000°C at 120 MPa in a vacuum. The heating rate was controlled as follows: from 20°C to 900°C at 100°C/min, from 900°C to 980°C at 20°C/min and from 980°C to 1000°C at 5°C/min. The holding time at 1000°C was 5 min.

The coated film neither contains cracks nor peels off. The bonding between the hydroxyapatite and consolidated MWNT seemed to be good, resulting from the SEM observation.

PO8

Preparation of Single-Walled Carbon Nanotube Solids by Spark Plasma Sintering method and Their Mechanical Properties

Go YAMAMOTO, Toru TAKAHASHI, Mamoru OMORI, Toshiyuki HASHIDA

Fracture and Reliability Research Institute, Tohoku University

1. Introduction

Many potential applications such as high-strength composites, field emission display, hydrogen storage media and drug carriers have been proposed for single-walled carbon nanotubes (SWCNTs). For biomedical applications such as artificial joint and dental implant, it is necessary to produce microscopic solid structures composed of SWCNTs that possess both the biocompatibility and mechanical compatibility with existing born. In our previous report, we have successfully prepared SWCNT solids without any additives using the spark plasma sintering (SPS) method, and the effect of processing conditions on mechanical properties and microstructures were investigated. Transmission electron microscopy (TEM) observations suggested that the graphite-like materials in the SWCNT solids increased with the increasing processing temperature and pressure. We supposed that the structure of SWCNTs may change into a graphite-like material due to the high-energy plasma generated in the SPS apparatus. The formation of graphite-like materials may impede the preparation of the SWCNT solids that possess intrinsic properties of SWCNTs. In this report, in order to examine the effect of processing method on the mechanical properties and microstructures, the SWCNT solid was prepared by hot-pressing.

2. Experimental

The starting materials were SWCNTs synthesized by using the arc discharge method, and purified by using a heat and chemical procedure. The SWCNT solids were prepared by SPS and hot-pressing in a graphite die with a diameter of 20mm at a temperature of 1000°C under a pressure of 120 MPa. The prepared specimens were disk-shaped about 20 mm in diameter and 1.5 mm in thickness. The

specimens were cut using a SiC saw and polished with Emery paper into 20×2×1 mm pieces.

The mechanical properties of the SWCNT solids, the Young's modulus, fracture strength and fracture energy were measured by three-point bending tests, which were performed on a universal testing machine in atmospheric conditions at room temperature. The load application was performed at a crosshead speed of 0.05 mm/min. The Young's modulus E_b, fracture strength σ_b and fracture energy G_b are given by the following equations

$$E_b = \frac{1}{4} \cdot \frac{L}{bh^3} \cdot \frac{P}{\delta} \tag{1}$$

$$\sigma_b = \frac{3P_bL}{2bh^2} \tag{2}$$

$$G_b = \frac{J_b}{A} \tag{3}$$

where L is span length, b the specimen width, h the specimen thickness, P/δ the initial liner slope of the load-displacement curve, P_b the maximum load, J_b the total area under the load-displacement curve, and A the cross-sectional area of the specimen. Three specimens were tested for both processing method. Microstructural observations were carried out using TEM and Raman spectroscopy.

3. Results and discussion

Typical load-displacement curves for the SWCNT solids are shown in Fig. 1. In both case, the load increases until it reaches the peak load. A rapid crack extension was observed just after the peak load followed by a long tail. Therefore, the fracture response of SWCNT solids may be categorized as a quasi-brittle material, regardless of the processing method. In addition, it can be seen that the maximum load of the SWCNT solid prepared by SPS was higher than that of SWCNT solid prepared by hot-pressing.

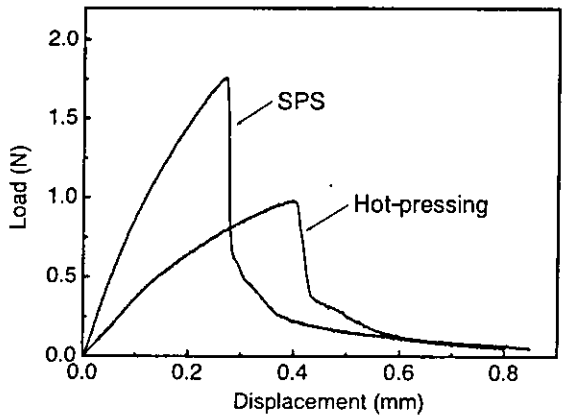

Figure 1. Typical load-displacement curves for the SWCNT solids

The physical and mechanical properties for the both specimen are shown in Table 1. The bulk

density of the specimen prepared by SPS was slightly larger than that of the specimen prepared by hot-pressing. However, the Young's modulus and fracture strength of the specimen prepared by SPS are, respectively, about three and two times higher than that of specimen prepared by hot-pressing. The specific modulus and specific strength of the SPS specimens were 16.7 GPa/Mg/m^3 and 16.9 MPa/Mg/m^3, respectively. On the other hand, the values of the hot-pressed specimens were 5.6 GPa/Mg/m^3 and 8.3 MPa/Mg/m^3, respectively.

Figure 2(a) shows a typical low magnification TEM photograph of the fracture surface for the

Table 1. The physical and mechanical properties for the SWCNT solids prepared by SPS and hot-pressing, respectively.

Processing method	Bulk density ρ (Mg/m^3)	Young's modulus E_b (GPa)	Fracture strength σ_b (MPa)	Fracture energy G_b (N/mm)
SPS	1.41	23.6	23.8	0.21
Hot-press	1.39	7.8	11.6	0.16

specimen prepared by SPS. From the morphology of the fracture surface, extensive pull-out of SWCNT bundles of approximately 1μm in length were observed, and the diameter of SWCNT bundles was observed to decrease toward their tips. In the case of hot-pressing, morphology of the fracture surface was similar to that seen in Fig. 2(a). Figure 2(b) and (c) show the high-resolution TEM photographs of the fracture surface of SWCNT solids prepared by (b) SPS and (c) hot-pressing, respectively. From the TEM photographs, it can be seen that for both case, numerous bundles containing 10-30 nanotubes protrude from the fracture surface. This observation suggests that the SWCNT bundles form a nano-sized structure in the SWCNT solids. Detailed observation of the fracture surface indicates that no breakage of SWCNTs occurred in the bundles, suggesting that the detachment between the bundles may be a controlling factor in the fracture process of the SWCNT solids. It is noted that the outer surface of the bundle in SPS specimen is much rather than in hot-pressed specimen.

To obtain an in-depth understanding of the composition of SWCNTs in the samples, the SWCNT solids were characterized using Raman scattering. It is well known that the Raman intensity ratio I_G/I_D of the peaks 1350 cm^{-1} (D-band) and 1590 cm^{-1} (G-band) is a good index for the evaluation of the SWCNTs abundance. Figure 3 shows the Raman intensity ratio I_G/I_D of the SWCNT solids. For the sake of comparison, the previous results are also shown in Fig. 3. Here, the I_G/I_D was normalized using the previous results of solidified by mechanical compaction only at room temperature (I_G/I_D=70). It can be seen that the abundance of SWCNTs in the specimen was sensitive to the processing method. In addition, the I_G/I_D of the specimen prepared the hot-pressing was larger than that of specimen prepared by SPS. The reason for this result may be due to the high-energy plasma generated in the SPS apparatus. The SPS apparatus is

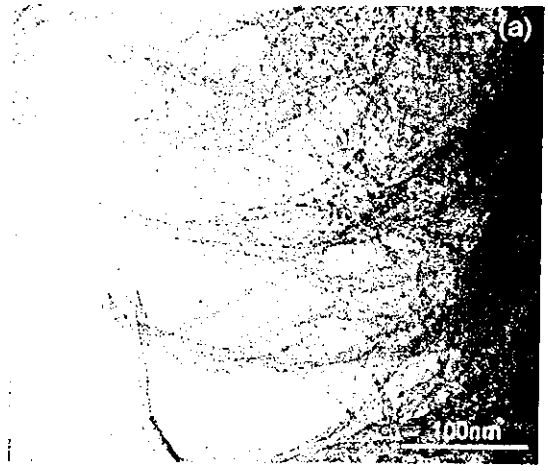

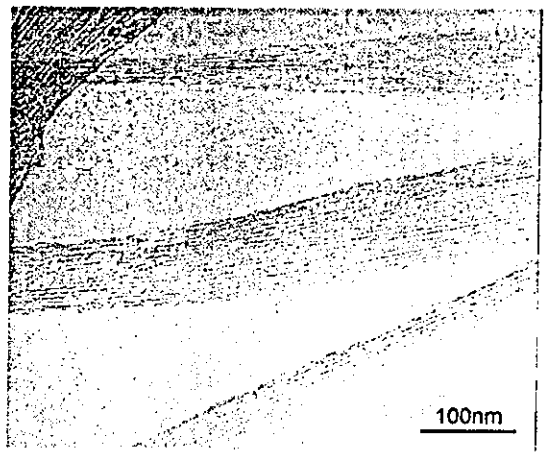

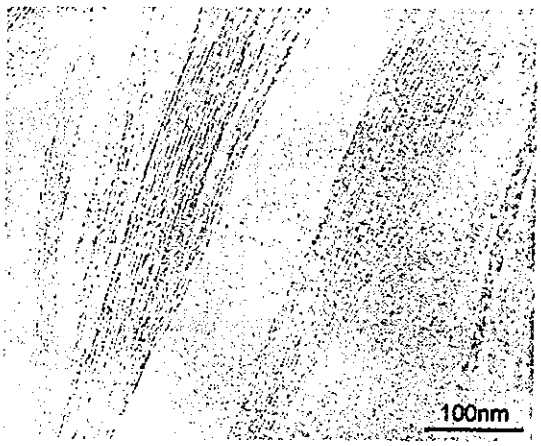

Figure 2(a) shows the typical low magnification TEM photograph of the fracture surface for the specimen prepared by SPS. The high-resolution TEM photograph of the fracture surface of SWCNT solids prepared by (b) SPS and (c) hot-pressing, respectively.

equipped with gaps between the two electrodes in the electric discharge machine, and high-energy plasma is generated there. We expect that the SWCNTs have suffered damage in the course of SPS. In contrast, we have successfully prepared SWCNT solids employing the hot-press method. The method may allow us to further develop a technique in order to mitigate the process induced damage, and to improve the mechanical properties of SWCNT solids.

4. Conclusions

The main results obtained from this study can be summarized as follow:

1. We have successfully prepared SWCNT solids without any additives using the hot-pressing at a temperature of 1000°C under a pressure of 120 MPa.

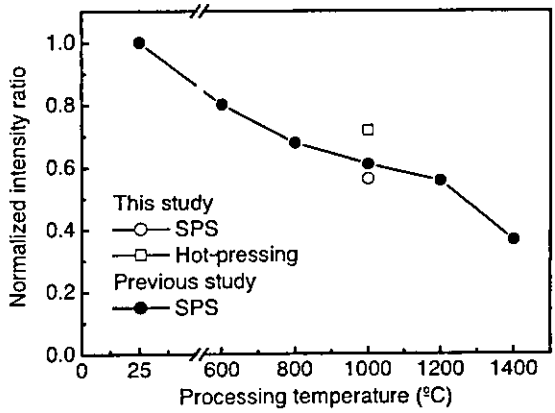

Figure 5. Raman intensity ratio of SWCNT solid as a function of processing temperature.

2. The SWCNT solids prepared by SPS and hot-pressing showed quasi-brittle fracture behavior. The Young's modulus and fracture strength of the SPS specimen were 23.6 GPa and 23.8 MPa, respectively. These values were about three and two times higher than that of the hot-pressed specimen.
3. TEM observations revealed that the failure of specimen occurred via inter-bundles slippage rather than fracture within the SWCNTs for both case. It may be possible to improve the mechanical properties of the SWCNT solids by introducing the stability of the links between SWCNTs within and between the bundles.
4. Raman scattering measurements revealed that the abundance of SWCNTs in the specimen prepared by hot-pressing was larger than that of the specimen prepared by SPS. The generated high-energy plasma in the SPS apparatus may damage the structure of SWCNTs compared with hot-pressing.

PO9

Synthesis and Size Classification of Metal Oxide Nanoparticles for Biomedical Applications

T. Atsumi[a], B. Jeyadevan[a], Y. Sato[a], K. Tamura[b], S. Aiba[c] and K. Tohji[a]

[a]Graduate School of Environmental Studies, Tohoku University 6-6-20, aramaki-aza aoba, aoba-ku Sendai, Japan, 981-8535

[b]Graduate School of Dental Medicine, Hokkaido University, kita13 nishi7, kita-ku, Sapporo, Japan, 060-8586

[c]Graduate School of Medicine, Tohoku University,1-1 seiryou-machi, aoba-ku, Sendai, Japan, 980-8574

ABSTRACT

Magnetic nanoparticles are considered for biomedical applications, such as the medium in magnetic resonance imaging, hyperthermia, drug delivery, and for the purification or classification of DNA or virus. The performance of magnetic nanoparticles in biomedical application such as hyperthermia depends very much on the magnetic properties, size and size distribution. We briefly described the basic idea behind their use in drug delivery, magnetic separation and hyperthermia and discussed the prerequisite properties magnetic particles for biomedical applications. Finally reported the synthesis and classification scheme to prepare magnetite (Fe_3O_4) nanoparticles with narrow size distribution for magnetic fluid hyperthermia.

Keywords: magnetite, hyperthermia, ferrite, magnetic fluid, size, size distribution, size classification

1. Introduction

Magnetic materials have long been of interest in biomedical applications including magnetic resonance imaging (MRI) for clinical diagnosis, magnetic drug targeting, hyperthermia anti-cancer strategy, and enzyme immobilization[1-6]. However, the use of magnetic nanoparticles depend upon the biocompatibility and sensitivity of these materials, beside other specific properties such as size, size distribution, dispersability in saline, etc. Though considerable work has been done to look into the possibility of using magnetic iron oxide particles in various biomedical applications, little has been done to determine the appropriate size and size distribution of the same for any specific application. And also, while the biocompatibility of magnetic iron oxide has been proved, no effort has been made to study the biocompatibility of magnetic particles with enhanced magnetic properties such as metals and alloys. In this paper, we discuss the possible use of magnetic particles in biomedical applications, prerequisite properties of magnetic particles in general and specific to hyperthermia and finally experimental approach towards the preparation of magnetic particles for magnetic fluid hyperthermia.

2. Biomedical applications

The use of magnetic particles has already been proposed for various biomedical applications and the area of applications is also on the rise. Here, we briefly describe the basic idea behind their use in drug delivery,

magnetic separation and hyperthermia.

2.1 Drug delivery

In drug delivery, biocompatible magnetic nanoparticles are injected as a drug-carrier to the patient via circulatory system. The drug would be attached to a surface coating on the particles such as dextran, PVA, polyglycols etc. The drug-carrier is concentrated at the target using external magnetic field and released by changing the physiological conditions such as blood flow rate, pH, protein or temperature[7]. The parameters viz., magnetic field strength, amount of particles and drug, magnetic properties of particles and method of release play a major role for high therapeutic effect. Besides the localizability of the particles, the immobilization of a signal molecule on the particles may protect it from degradation to some extent and the long term binding to a receptor may lead to the activation of the receptor for long periods. Thus, the use of nanoparticles may prove to be a very efficient method of delivering a drug to a cell. There are two possible events; the one usually reported is the endocytosis of the particles after preliminary capture at the surface of the cell. The other, discovered only recently is that if certain protein coatings attached to the particles, endocytosis is prevented. Here the proteins have to be bound by surface receptors. This is not in itself a disadvantage in many situations as large number of drug receptors are located at the cell surface and since one of them can be chosen to bind the particle to a surface receptor irreversibly and another can be attached to the first to be the active drug which will attach to a nearby second receptor. In total, the use of magnetic particles for such application is considered very promising and could be realized in the near future.

2.2 Magnetic separation

The basic concept of magnetic separations in biomedical applications is to bind selectively the biomaterial of interest, such as a specific cell, protein or DNA fragments, to a magnetic particle and then separate it from the surrounding matrix using a magnetic field for the manipulation or purification of biological cells/molecules. Magnetic beads of iron oxide (gamma-Fe_2O_3 and Fe_3O_4) with diameters ranging from a few nanometers to a few micrometers are typically used for such separations. In magnetic fluids, the particle sizes are less than 10 nm and exhibit superparamagnetic behavior. These particles will magnetize under a strong applied magnetic field, but retaining no permanent magnetism once the field is removed. This on/off switching behavior is a particular advantage in magnetic separation and well established as a viable alternative to centrifugal separation of chemical or biological solutions. Magnetic separation using biocompatible magnetic nanoparticles is a two-step process, involving (i) the tagging or labeling of the desired biological entity with magnetic material, and (ii) the separating out of these tagged entities via a fluid based magnetic separation device. Tagging is made possible through the modification of the surface of the magnetic nanoparticles, usually by coating with biocompatible molecules such as dextran, polyvinyl alcohol, and phosopholipids[8-11]. The magnetically labeled material is separated from its native solution by passing the fluid mixture through a region in which there is a magnetic field gradient, which can immobilize the tagged material via the magnetic force. Chemical modified particles and many kind of biological entities mixed and separate specific biological entities using magnet from their native environment[12-14]. In addition, ferromagnetic as well as superparamagnetic particles coated or encapsulated with polymers or liposome can be used for magnetic labeling. This use of magnetic particle in this field of application is gaining momentum

2.3 Hyperthermia

Hyperthermia (also called thermal therapy or thermotherapy) is a type of cancer treatment in which body tissue is exposed to high temperatures (up to 42°C). Research has shown that high temperatures can damage and kill cancer cells, usually with minimal injury to normal tissues; (1) by killing cancer cells and damaging proteins and structures within cells and (2) hyperthermia may shrink tumors. Though the idea of magnetic hyperthermia has been proposed long time ago, recently a lot of researchers have begun to show interest. The magnetic nanoparticles for hyperthermia are divided into two main classes; ferromagnetic or ferrimagnetic (FM) particles and superparamagnetic (SPM) particles. Each particle has its own advantages and disadvantages in heat generating mechanism. In the case of FM particles the amount of heat generated per volume (P_{FM}) is given by the frequency multiplied by the area of the hysteresis loop:

$$P_{FM} = \mu_0 \; f \; \oint H \, dM$$

Where, μ_0 is the magnetic permeability of free space, H, magnetic field and M is the magnetization. For FM particles there is no implicit frequency (f) dependence in the integral of the above equation. That is amount of heat depends on the magnetic properties of nanoparticles.

Recently, the use of eddy current loss for hyperthermia has also been considered[15]. Here, the magnetic substance is coated with a metal layer of few tens to few hundreds of nanometer thick. When an alternating magnetic field is applied to the composite, eddy current loss is generated. However, when the temperature of the composite rises above the Curie temperature (Tc) of the magnetic substance, the magnetic substance does not retain its magnetic property and eddy current loss is not generated. This method has an advantage over the rest of the methods as the maximum temperature generated could be manipulated by selecting the magnetic material with specific Curie temperature.

Another method that has drawn interest nowadays is the magnetic fluid hyperthermia (MFH) using SPM nanoparticles dispersed in polar or non-polar solvents[16-18]. The generation of heat (P_{SPM}) by the SPM particles under AC magnetic field has been derived to be as follows[19].

$$P_{SPM} = \mu_0 \; \pi \; f \; \chi'' \; H^2$$

which can be interpreted physically as meaning that if M lags H there is a positive conversion of magnetic energy into internal energy. This simple theory compares favorably with experimental results, for example, in predicting a square dependence of SPM on H and the dependence of χ'' (magnetic susceptibility) on the driving frequency[20,21]. Considering the operational constraints in magnetic field strength and frequency, superparamagnetic particles are more likely to offer useful heating than the ferromagnetic counterpart. Between the relation of frequency and particles size, relaxation, that is, generating heat depends very much on size and size distribution in specific frequency.

3. Prerequisite properties of magnetic particles for biomedical applications

The magnetic particles are preferred very much in biomedical applications over the other non-magnetic materials as they can be detected and manipulated from outside. However, to take advantage of this, the particle should possess enhanced magnetic property, such as high magnetization. Magnetic nanoparticles are classified generally into three categories, viz., pure metal nanoparticles like Fe and Co, alloy nanoparticles like FeCo and FePt and

metal oxide particles like magnetite (Fe_3O_4) and cobalt ferrite ($CoFe_2O_4$). In this context, either metal or alloy magnetic particles has higher magnetization over their oxides. Though the metal and alloy particles are superior in their magnetic properties, they are very unstable in the oxidizing atmosphere. However, the technology to coat these particles with either magnetic oxide or non-magnetic layer have been proposed. Thus, the biocompatibility of magnetic oxides and other non-magnetic oxide layers such as silica limits their use in biomedical applications. Considerable research has been carried out in determining the biocompatibility of magnetic iron oxides, however, the potential of highly magnetic metal and alloy particles is an area that needs consideration.

Considering the biological/biomedical interest of these nanoparticles, the controllable sizes ranging from few nanometers to tens of nanometers, which places them at dimensions that are smaller than or comparable to those of a cell (10-100 micron), a virus (20-450 nm), a protein (5-50 nm) or a gene (2nm wide and 100 nm long) and allow them to get close to a biological entity of interest[16]. The suitable particle diameter for biomedical application is another area, which needs to be studied. Though there are conflicting reports, no systematic work has been done in this area. To begin with, it is essential to use magnetic iron oxide particles with different diameters to determine the operational range. However, the chemical methods available at our disposal do not facilitate the synthesis of particles with narrow size distribution. Thus, the size classification techniques at nanosize level have to be coupled with the synthesis to arrive at particles with narrow particle size distribution.

On the other hand, some applications itself limit the size of the particles to be used in biomedical applications. For example, the magnetic fluid hyperthermia (MFH), where magnetic particle dispersion is injected into cancer cells exerts heat under alternating current external magnetic field. To get optimum efficiency in MFH, the nanoparticles must have specific size and narrow size distribution. This means that the particles size and size distribution is dictated by the application itself rather than the biological constraints. Rosensweig has considered the use of maghemite, magnetite, cobalt ferrite and barium ferrite particles for hyperthermia and evaluated the heat generation efficiency[19]. When the use of such materials is considered for biomedical applications, the primary concern is the biocompatibility of the same. Among the materials listed above magnetite and maghemite have already been reported to be biocompatible. Furthermore, the dispersability of these materials in saline has been proved possible using double layered ionic surfactants in the cases of maghemite, magnetite and cobalt ferrite[22]. Though the heat efficiency of the above materials has been proved theoretically, the most practicable material has been found to be magnetite for its critical size of 13 nm. Though maghemite can also be considered, preparing the dispersion using the critical size of around 21 nm is considered difficult. Considering the above facts, the synthesis of magnetite particles with 13 nm in diameter becomes important to obtain the maximum heat efficiency at a frequency of 300 kHz and magnetic field of 0.9 T. In general, the heat generated is very sensitive to the particle diameter and particles with narrow size distribution are very important. Hence, the preparation of magnetite nanoparticles dispersion with narrow size distribution is very important to optimize the heat efficiency. Therefore in the next section, we discuss about the synthesis and size classification at nanosize level will be discussed.

4. Preparation of magnetic iron oxide for hyperthermia

4.1 Synthesis of magnetite nanoparticles

The magnetite nanoparticles for the magnetic fluid hyperthermia was prepared by coprecipitation method. However, as the appropriate size of the particles for heat generation is around 13 nm, which is higher than the average diameter of the particles synthesized by coprecipitation method, the synthesis was attempted using two types of alkali solvents, namely NaOH and NH_4OH. The ferrous ($FeSO_4 \cdot 7H_2O$) and ferric chloride ($FeCl_3 \cdot 6H_2O$) with mole ratio of Fe(III)/Fe(II) = 2 were dissolved in distilled water and either NaOH or NH_4OH solution was introduced until the *p*H of the mixture reached 12. The reaction was carried out at 25 °C and the mixture was stirred for 30 minutes. The precipitate was recovered and washed with distilled water. Then, the surface of these particles were coated with oleic acid and dispersed in isoparaffin and heated at 100 °C for 1 hour to produce the magnetic fluid. The magnetic fluids prepared by using NaOH and NH_4OH are named as NaOH-Fe_3O_4 and NH_3-Fe_3O_4 respectively. The magnetic particle synthesis scheme is given in Fig. 1. The TEM micrographs of these particles are shown in Fig. 2(a) and Fig. 3(a). The average size and size distribution of the particles synthesized by coprecipitation method using NaOH was smaller than the one synthesized with NH_4OH. The size distribution, average diameter and the standard deviation of each sample were evaluated by considering a population of 400 particles from the representative TEM photographs. Size distribution results and TEM photographs show in Fig. 2 and Fig. 3. The average diameter of the particles synthesized using NaOH was 10.0 nm, whereas the ones synthesized using NH_4OH was 10.8 nm. It is believed that the difference in the alkalinity between NaOH and NH_4OH was the reason for the variation in average particle diameter. As NH_4OH is a weak base, rise in the *p*H of the solution is rather slow compared to NaOH. Thus, this may have caused a difference in the nucleation stage, resulting in comparatively smaller number of nucleus in the NH_4OH case. Consequently leading to particles with diameters marginally larger than that of the NaOH case.

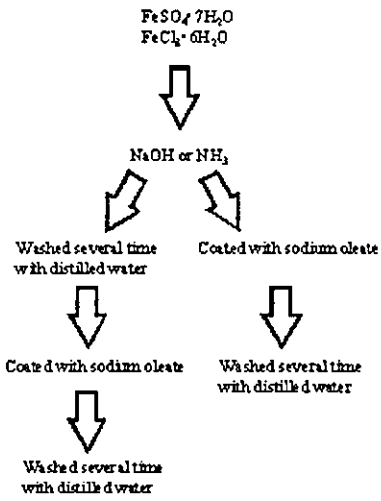

Fig. 1 Schematic diagram for magnetite nanaoparticles synthesis

4.2 Size classification and characterization

The size classification at nanosize level was carried out under premise that the diameter of the particles coated with a surfactant depends on the interparticle separation distance. This can be achieved either by coating the particles with surfactants of different chain length or bringing the particles coated with surfactant and dispersed in an organic medium such as toluene in contact with bad solvents such as acetone. In the latter case, the interparticle distance is reduced by the contraction of the hydrophobic tail caused by introduction of the bad solvent. Depending on the degree of contraction, which is a function of the concentration of the bad solvent, the diameter of the particles that undergo size selective coagulation will be decided[22]. The particles with critical diameter (Dc) will coagulate and settle to the bottom of the vessel while the particles with diameter less Dc will remain in suspension. The particle that remained in suspension can be made coagulate by increasing the